Resonant multiple Auger decay after the $2p_{3/2}^{-1}$ $4s$ excitation in Ar studied with a multielectron coincidence method

Y. Hikosaka,[1] P. Lablanquie,[2,3] F. Penent,[2,3] P. Selles,[2,3] E. Shigemasa,[4] and K. Ito[5]
[1]*Department of Environmental Science, Niigata University, Niigata 950-2181, Japan*
[2]*UPMC, Université Paris 06, LCPMR, 11 rue Pierre et Marie Curie, 75231 Paris Cedex 05, France*
[3]*CNRS, LCPMR (UMR 7614), 11 rue Pierre et Marie Curie, 75231 Paris Cedex 05, France*
[4]*UVSOR Facility, Institute for Molecular Science, Okazaki 444-8585, Japan*
[5]*Photon Factory, Institute of Materials Structure Science, Oho, Tsukuba 305-0801, Japan*
(Received 30 October 2013; published 10 February 2014)

The multiple Auger electron emission processes after the $2p_{3/2}^{-1}$ $4s$ excitation in Ar have been investigated with a multielectron coincidence method. We have observed the double, triple, and quadruple Auger decays of the resonant state, where both cascade and direct processes are identified. The cascade processes in the resonant double and triple Auger decays result mostly from the spectator behavior of the Rydberg electron in the initial core-hole decay: First Auger decay produces ion states with large internal energies, and subsequent electron emission leads mainly formation of ground Ar^{2+} and Ar^{3+} states. It is revealed that spectator behavior, which is known to be the dominant path in resonant single Auger decay, is also important in the direct paths of the resonant double and triple Auger decays. In contrast, the participation of the Rydberg electron is predominant in the direct path of the resonant quadruple Auger decay.

DOI: 10.1103/PhysRevA.89.023410 PACS number(s): 32.80.Hd, 32.80.Fb, 32.80.Rm

I. INTRODUCTION

X-ray absorption can promote a core electron of an atom to a Rydberg orbital. The core-to-Rydberg resonance state usually decays by emitting Auger electron(s). The understanding of the resonant Auger decay mechanism has been developed mainly by conventional electron spectroscopy, but is largely limited to the process of single Auger electron emission. On the other hand, mass spectrometry has shown that resonant Auger decay includes, with a considerable fraction, processes associated with the emission of two or more electrons, when such multiple Auger processes are energetically allowed [1,2].

Resonant single Auger (RSA) decay processes can be clarified in terms of spectator and participator behavior of the Rydberg electrons [3], where the spectator process is strongly favored. If the Rydberg electron were exclusively spectator even in the resonant multiple Auger decay, the Auger decay pathways would be similar to those in the normal Auger decay of the corresponding core-hole state after the inner-shell ionization. In such case, one could expect the final charge state distribution due to the resonant Auger decay to mimic the one due to the normal Auger decay, with a shift of one charge due to the presence of the spectator Rydberg electron. However, a large deviation from this expectation is usually observed. For example, while the final charge state distribution formed after $2p$ ionization from Ar is Ar^{2+}:Ar^{3+} = 1:0.11 [4], the distribution at the $2p^{-1}$ $4s$ excitation is Ar^{+}:Ar^{2+} = 1:0.46 [5]; here, emission of two Auger electrons is four times more favorable in the resonant Auger decay. Therefore, it may be anticipated that a Rydberg electron is not simply a spectator in resonant multiple Auger decay; however, no detailed view has been established about the behavior of a Rydberg electron in resonant multiple Auger decay.

A comprehensive understanding of the multiple Auger decay mechanism of core-excited atoms can be obtained by coincidence detection of all the emitted Auger electrons in the full energy range. Such a challenging coincidence investigation can be effectively realized by the use of a magnetic-bottle-type electron spectrometer [6], as demonstrated in our previous study on the simultaneous two-electron emission upon $2p$ core excitation in Ar [7]. We apply here this method to the study of all multiple Auger decay routes of the $2p_{3/2}^{-1}$ $4s$ resonance state in Ar. The electron coincidences corresponding to resonant double Auger (RDA), resonant triple Auger (RTA), and resonant quadruple Auger (RQA) decays are identified, and the energy correlation information on the individual decay paths enables us to clarify the behavior of the Rydberg electron in the resonant multiple Auger decay processes.

II. EXPERIMENT

The experiments were performed at the undulator beamline BL-16A of the Photon Factory. Single bunch operation of the storage ring provided a 624-ns repetition period for the 200-ps-width light pulses. Synchrotron radiation was monochromatized by a grazing incidence monochromator using a varied-line-spacing plane grating and the photon bandwidth was set to 30 meV. A mechanical chopper [8] was used to increase the light-pulse period to 12.5 μs thus allowing the electron's absolute time-of-flight determination. Multicoincidences were recorded between electrons, analyzed in energy by their times of flight in a magnetic-bottle electron spectrometer [6]. The descriptions of the spectrometer and of the data accumulation scheme are given elsewhere [8]. Conversion of the electron time of flight to energy was achieved by measuring Ar photoelectron lines at different photon energies. The energy resolving power of the apparatus, $E/\Delta E$, was nearly constant at 60 for electrons of $E > 3$ eV, though ΔE was limited to around 20 meV (full width at half maximum) for $E < 1$ eV. It was estimated that the electron detection efficiency oscillates, as a function of electron energy, between 65% and 75% in the electron energy range below 300 eV. A multielectron coincidence dataset was accumulated

on the $2p_{3/2}^{-1}\,4s$ resonance (at a photon energy of 244.39 eV) in Ar, with a count rate around 2 kHz during an accumulation time of 12 h. For this count rate, considering the light-pulse repetition rate (80 kHz), the possibility that two different ionization events occur in a single light pulse is estimated to be 2.5% at most. This contribution of random coincidences is expected to be minor in the accumulated coincidence dataset, compared to the double Auger decay probability of the $2p_{3/2}^{-1}\,4s$ resonance state that is reported to be 30% [5]. Moreover, these random coincidence events will appear mainly in a zone which is outside the true coincidence region, because the majority of the incoming electrons results from single Auger decay and has a larger kinetic energy (over 180 eV) than those of the electrons associated to the double Auger decay. Actually, we find only a negligible contribution from random coincidences in two electron coincidence spectra, and none in higher coincidence spectra.

III. RESULTS AND DISCUSSION

A. Spectra for resonant Auger decay of Ar $2p_{3/2}^{-1}\,4s$

Figure 1 shows a histogram of the energies of all the electrons and those of the energy sums of two, three, and four electrons detected in coincidence, derived from the coincidence dataset accumulated at the $2p_{3/2}^{-1}\,4s$ resonance in Ar. These spectra exhibit essentially the electronic states of the individual ions produced by the resonant Auger decay, while minor contributions from valence multiple photoionization should be included. It is estimated from the partial photoionization cross section curves [5] that valence photoionization contributes to about 15% and 7% of the intensity in Figs. 1(a) and 1(b), while its contribution is negligibly small in Figs. 1(c) and 1(d). Note that Ar^{5+} is also energetically accessible from this resonance, but there has been no mass spectrometric report on the Ar^{5+} production at the resonance and the corresponding quintuple coincidences could not be identified in the coincidence dataset.

The RSA spectrum in Fig. 1(a) shows sizable formation of Rydberg-excited Ar^{+*} states in the Auger electron's energy range of 170–210 eV. These Ar^{+*} states are populated through spectator RSA processes [9,10]. Their intensity is much stronger than that of the $3p^{-1}$ and $3s^{-1}$ formations which could be associated with participator processes in the RSA decay but are actually due dominantly to valence photoionization. Such a preference of spectator processes with respect to participator ones is commonly observed in RSA decay. In contrast, the other spectra due to multiple Auger paths show large populations of the low-lying levels with no Rydberg excitation. The formation of these low-lying levels apparently needs participation of the Rydberg electron in the multiple Auger processes. However, as shown later, thorough inspection of the correlations of the Auger electrons' energies reveals that spectator behavior of the Rydberg electron is also dominantly important in these multiple Auger decay paths.

B. Resonant double Auger decay

Figure 2 displays the energy correlation map for two Auger electrons emitted in the RDA decay, which is essentially the same as in Fig. 2 of [7] but with higher statistics. Here the

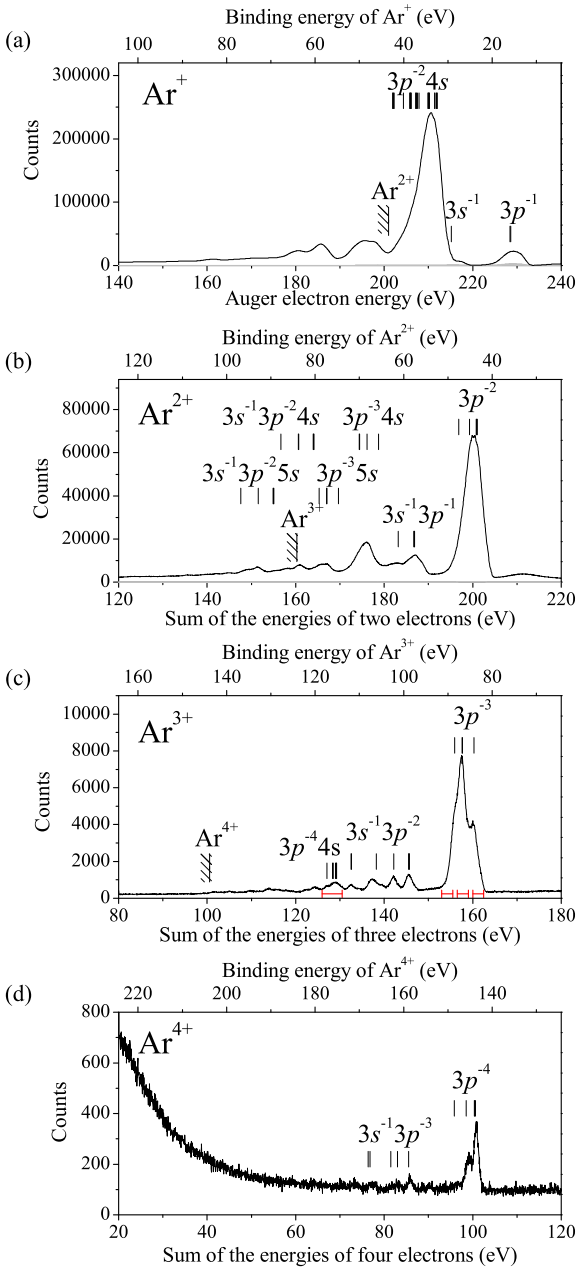

FIG. 1. (Color online) (a) Histogram of the energies of all the electrons, and those of the energy sums of (b) two, (c) three, and (d) four electrons detected in coincidence, derived from the coincidence dataset accumulated at the Ar $2p_{3/2}^{-1}\,4s$ state lying at 244.39 eV. The electronic states of the individual ions produced by the RSA (a), RDA (b), RTA (c), and RQA (d) decays are exhibited. The energy levels for the Rydberg-excited Ar^{2+} states, calculated from the reported Ar^{3+} levels [12] by the assumption of the quantum defects to be 1.45 [7], are indicated in (b). The other energy levels are from [12]. Four energy ranges for the extractions of the curves in Fig. 5 are indicated in (c).

intensity in the upper left area of (slow electron energy) > (fast electron energy) × 0.2 has been magnified by a factor of 20, in order to accentuate weak structures. In this plot, coincidence yields associated with the formation of a given Ar^{2+} final state necessarily fall onto a diagonal line defined

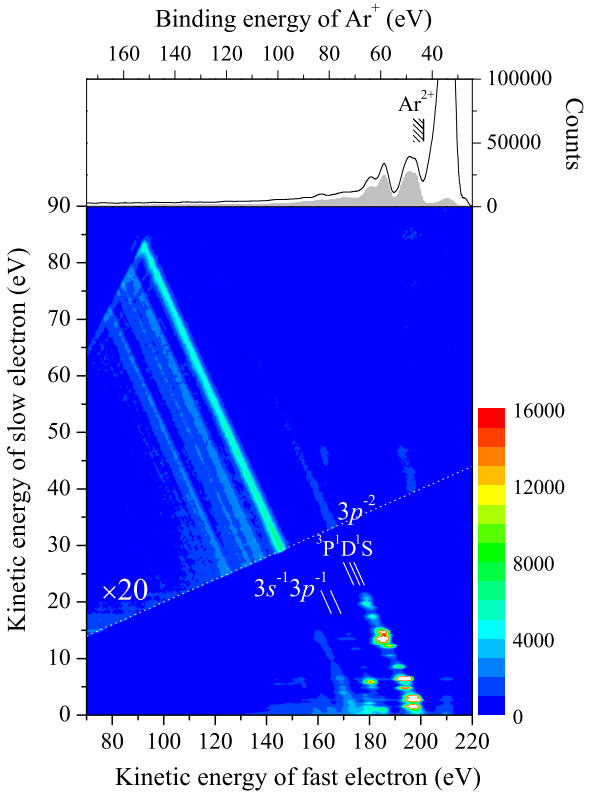

FIG. 2. (Color online) Energy correlation map for two Auger electrons detected in coincidences, where the intensity in the area of $y \geq x \times 0.2$ is magnified by a factor of 20. This map is essentially the same as in Fig. 2 of [7], but with higher statistics. The top panel shows the projection of the coincidence counts on the two-dimensional map onto the horizontal axis (shaded curve), compared to the RSA spectrum (solid line) in Fig. 1(a). In the projection curve, the small peak lying below the binding energy of the Ar^{2+} threshold is due to random coincidences. The peak intensity is about 2% of the corresponding peak in the RSA spectrum, and the spectral profiles above the Ar^{2+} threshold also should include a similar contribution from random coincidences.

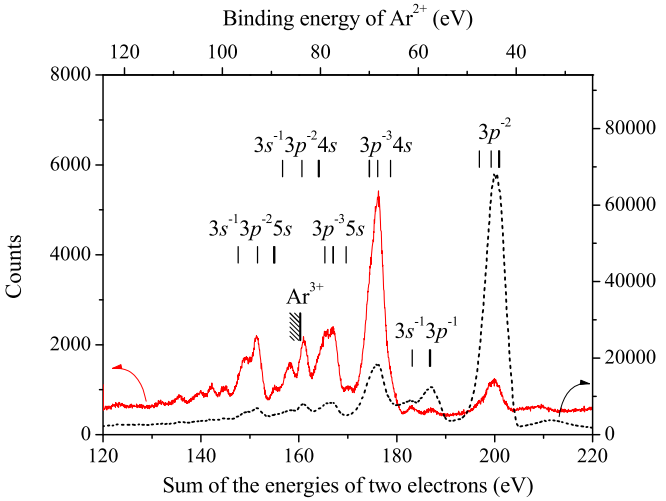

FIG. 3. (Color online) Histogram of the kinetic energy sum of the two Auger electrons (red solid), which is obtained for the magnified area in Fig. 2, thus by masking effectively the cascade RDA contribution, compared with a replot (black dotted) of the curve in Fig. 1(b). The energy levels for the Rydberg-excited Ar^{2+*} states are calculated from the reported Ar^{3+} levels [12], by assuming the quantum defects to be 1.45 [7].

by the energy conservation law: (slow electron energy) + (fast electron energy) = (photon energy) − (binding energy of the Ar^{2+} state). The spectrum in Fig. 1(b) thus corresponds to the integration of the coincidence counts on this map along the direction for (slow electron energy) + (fast electron energy) = const.

As the features seen on the two-dimensional map in Fig. 2 and the formation mechanism of the Ar^{2+} levels were already discussed in our former study [7], only a brief summary will be given here:

(1) Along the diagonal lines corresponding to the $Ar^{2+}\,3p^{-2}$ and $3s^{-1}\,3p^{-1}$ formations, intense spots, whose coordinates are defined by the discrete kinetic energies of the two Auger electrons, are exhibited in the fast Auger electron's energy range of 170–200 eV. These spots result from cascade RDA processes, and the fast Auger electrons depict the Ar^{+} states populated above the Ar^{2+} threshold.

(2) The magnified area on the energy correlation map exhibits several diagonal stripes on which no clear spot structure due to cascade RDA process is identified. These stripes originate from direct RDA decay in which two Auger electrons are emitted simultaneously and share continuously the available energies corresponding to the energy difference between the initial core-excited and the final Ar^{2+} states. The direct RDA processes mainly produce Rydberg-excited Ar^{2+*} states converging to Ar^{3+} levels.

The cascade RDA processes yielding the $Ar^{2+}\,3p^{-2}$ and $3s^{-1}\,3p^{-1}$ formations are constituted by spectator RSA decay into high-lying Ar^{+*} levels and their subsequent decay with slow electron emission into these Ar^{2+} states [7]. Thus the intensities of these cascade processes result from the spectator RSA decay of the core-excited state. It can be estimated from the features in Fig. 2 that the cascade process contributes about 60% to the total intensity of the RDA decay.

Figure 3 shows, in comparison with a plot of the curve in Fig. 1(b), the histogram of the kinetic energy sum of the two Auger electrons, which is obtained for the magnified area in Fig. 2 and thus by masking effectively the contribution of cascade RDA. This histogram remarkably exhibits structures corresponding to Rydberg-excited Ar^{2+*} states converging to Ar^{3+} thresholds, where minor promotions of the Rydberg electrons can be identified [7]. The formation of these Rydberg-excited Ar^{2+*} states is most naturally attributed to noninvolvement of the initial Rydberg electron in the RDA process; that is, the Rydberg electron behaves as a spectator of two-electron ejection from the ion core. We can attribute this process to the spectator path in the direct RDA decay, while the intensity of the $Ar^{2+}\,3p^{-2}$ formation includes the participator path in the direct RDA decay. It should be noted that the peak intensities in the histogram do not correctly reflect the Ar^{2+} populations via direct RDA decay, as the whole energy distributions of direct RDA decay, which rise steeply down to 0 eV, are not included here. In practice, the ratio between spectator and participant contributions in the direct RDA decay

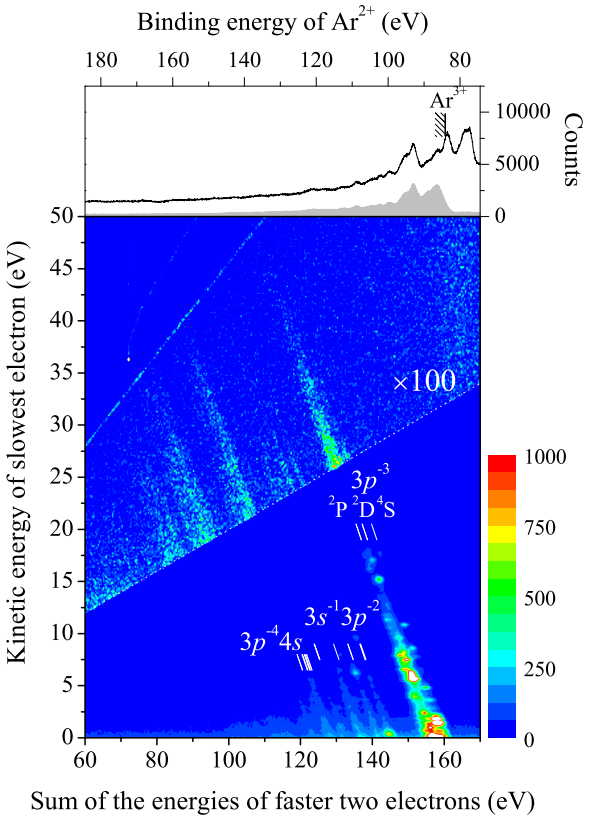

FIG. 4. (Color online) Energy correlation map displaying the triple coincidences for the RTA decay, where the coincidence yields are plotted as a function of the sums of the faster two electrons and of the kinetic energy of the slowest electron. The intensity in the area of $y \geq x \times 0.2$ is magnified by a factor of 100. The top panel shows the projection (shaded curve) of the coincidence counts on the two-dimensional map onto the horizontal axis, compared to the RDA spectrum (solid line) in Fig. 1(b). Contribution from random coincidences is not discernible here.

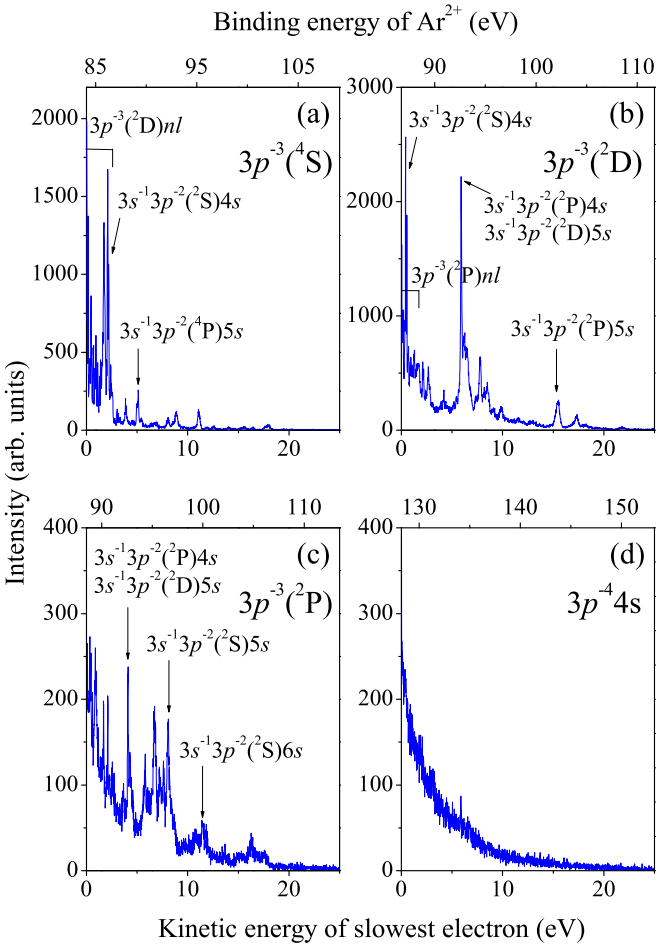

FIG. 5. (Color online) Energy distributions of slowest electrons emitted for the formation of the three components of Ar^{3+} $3p^{-3}$ and for that of Ar^{3+} $3p^{-4}$ $4s$, delineating the energies of Auger electrons emitted on the second steps in cascade RTA processes. The energy ranges set in the extraction of these distributions are indicated in Fig. 1(c).

is estimated to be about 4:1, from the electron yields for the whole energy distributions underlying the cascade RDA peaks, where the participant contribution corresponds to formation of low-lying states with no Rydberg excitation.

C. Resonant triple Auger decay

Part of the Rydberg-excited Ar^{2+} states seen in Fig. 3 lies above the Ar^{3+} threshold. These states can decay into lower-lying Ar^{3+} states, with the emissions of a third electron. The two-dimensional map in Fig. 4 displays the correlations in the triple coincidences. Here, the coincidence yields are plotted as a function of the sum of the kinetic energies of the two faster electrons, and of the kinetic energy of the slowest electron. Intensity in the area of (slowest electron energy) > (sum of the kinetic energies of the faster two electrons)×0.2 has been magnified. As indicated on this map, formation of Ar^{3+} levels appears along diagonal lines and thus the integration of the coincidence counts along the direction for (sum of the kinetic energies of the faster two Auger electrons) + (slowest electron energy) = const. corresponds to the spectrum in Fig. 1(c).

In the top panel of Fig. 4, the projection of the coincidence counts of the two-dimensional map onto the horizontal axis is compared with a partial plot of the Ar^{2+} spectrum shown in Fig. 1(b). The projection curve depicts the structure of the Rydberg-excited Ar^{2+*} states lying above the Ar^{3+} threshold. This observation indicates that the two faster Auger electrons in the triple coincidences are mostly emitted in the formation of Rydberg-excited Ar^{2+*} states through direct RDA decay, and the slowest electrons correspond mostly to the electron emission through autoionization of the Rydberg-excited Ar^{2+*} into lower-lying Ar^{3+}.

Figure 5 shows the intensity distributions along the diagonal lines for the formation of the three components of Ar^{3+} $3p^{-3}$ (^4S, ^2D, ^2P) and for that of Ar^{3+} $3p^{-4}$ $4s$, delineating the energies of the slowest Auger electrons emitted in the RTA processes. The electron energy ranges to select these Ar^{3+} final states are indicated in Fig. 1(c). Some intense peaks observed in Figs. 5(a)–5(c) are assignable to the $4s$ and $5s$ Rydberg states converging to the Ar^{3+} $3s^{-1}$ $3p^{-2}$ limits (see Fig. 5), by assuming their quantum defects to be around 1.5. In addition, the group of peaks below a kinetic energy of

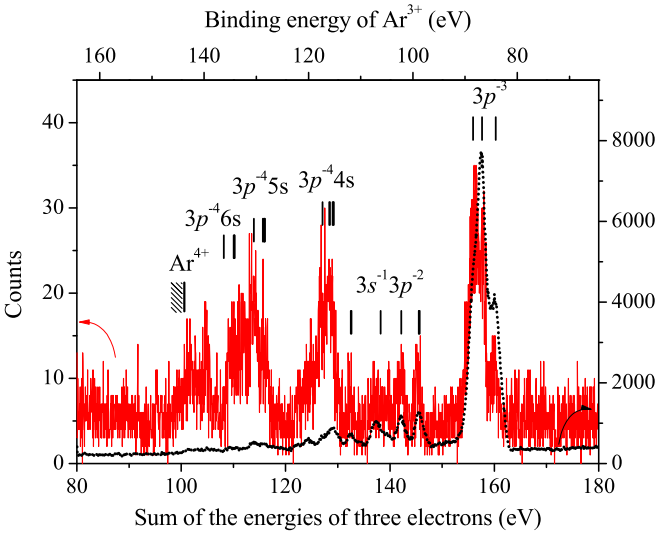

FIG. 6. (Color online) Histogram of the kinetic energy sum of the three Auger electrons (red solid), which is obtained for the magnified area in Fig. 4, thus by masking effectively the cascade RTA contribution, in comparison with a replot (black dotted) of the curve in Fig. 1(c). The energy levels for the Ar^{3+} $3p^{-4}$ $4s$ states are from [12], and the higher members are calculated with the same quantum defects.

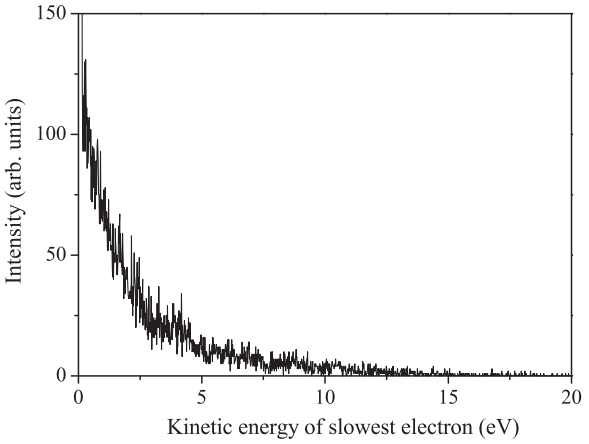

FIG. 7. Energy distribution of the slowest electrons in the quadruple coincidences for the formation of Ar^{4+} $3p^{-4}$.

2.6 eV in Fig. 5(a) and that below a kinetic energy of 1.7 eV in Fig. 5(b) are attributable to higher-n Rydberg states converging to the Ar^{3+} $3p^{-3}(^2D)$ and $3p^{-3}(^2P)$ limits, respectively. These cascade RTA paths after the formation of the high-lying Ar^{2+} states, which are due dominantly to the direct RDA decay of the core-excited state, are estimated to share in about 40% of the total RTA intensity.

One can see in the magnified area on the map in Fig. 4 several diagonal stripes on which no spot structures are visible. While it is expected that direct RTA decay produces such diagonal stripes on this map, all the intensities of the stripes cannot be readily ascribed to direct RTA processes. This is because cascade RTA processes, in which two electrons are simultaneously emitted and the third electron with a discrete kinetic energy is not the slowest electron, could contribute to the intensities of these stripes. However, it is likely that the contribution from such cascade RTA decay into the diagonal stripes is minor, because intermediate population of Ar^{2+} states lying in the range of >15 eV above the Ar^{3+} levels should be unfavorable. The histogram of the kinetic energy sum of the three Auger electrons, which is obtained for the magnified area in Fig. 4, is shown in Fig. 6, in comparison with the curve in Fig. 1(c). The intensities of the high-lying Ar^{3+} states are more pronounced, compared to those exhibited on the spectrum of the total triple coincidences. These high-lying Ar^{3+} states can be assigned to Rydberg-excited Ar^{3+*} states converging to Ar^{4+} states. It is likely that these Ar^{3+*} states are populated by direct RTA decay in which three Auger electrons are emitted simultaneously while the Rydberg electron remains a spectator. In practice, distinct peaks that could be associated with cascade processes are not visible in the energy distribution of the slowest electrons emitted in the Ar^{3+} $3p^{-4}4s$ formation [Fig. 5(d)] where the $4s$ electron is a spectator.

Similar to the direct RDA case, in the direct RTA decay, we attribute the formation of the Ar^{3+} $3p^{-3}$ and $3s^{-1}$ $3p^{-2}$ states to the participator path and that of the Rydberg-excited Ar^{3+*} to the spectator path. Comparing the features in Figs. 3 and 6, one sees that the participator contribution (formation of the low-lying states with no Rydberg excitation) is more sizable in the direct RTA decay than in the direct RDA decay. It is estimated that the ratio between spectator and participant contributions in the direct RTA decay is about 1:1.

D. Resonant quadruple Auger decay

In Fig. 6, the Rydberg-excited Ar^{3+*} populations due to the spectator RTA path rarely appear above the Ar^{4+} threshold, in contrast to the observation in the RDA case (shown in Fig. 3). This is due to the larger-term values in Ar^{3+} Rydberg states than in Ar^{2+} ones. Therefore, cascade RQA processes which result from the formation of Rydberg-excited Ar^{3+} and their subsequent decay are weak processes. In practice, no definite peak is seen in the electron distribution of the slowest electrons emitted in the formation of Ar^{4+} $3p^{-4}$ (see Fig. 7).

In Fig. 1(d), apart from the Ar^{4+} $3p^{-4}$ and $3s^{-1}$ $3p^{-3}$ states, no tangible feature can be ascribed to Rydberg-excited Ar^{4+*} states. Therefore, the direct RQA decay is induced mostly by the participation of the Rydberg electron, and the emission of four Auger electrons from the ion core, while keeping the Rydberg electron, is a minor contribution in the direct RQA path. While the present work identified fourfold coincidences corresponding to the RQA decay, the quadruple Auger decay after the Ar $2p$ ionization could not be detected with the use of the multielectron coincidence method [11]. This fact may suggest that the RQA decay is much more favorable than the quadruple Auger decay of the $2p$ core hole. This supposition is reasonable, because most of the RQA intensity is due to participation of the Rydberg electron.

E. Ion charge state distribution

The ratio of the final ion charge states after resonant Auger decay of the $2p_{3/2}^{-1}$ $4s$ resonant state can be estimated from the electron yields in Fig. 1, where the yields above the

thresholds of the upper ion formation are excluded because the corresponding states escape through subsequent electron emission, as has been revealed by the energy correlation analyses. The ratio is determined to be Ar^+:Ar^{2+}:Ar^{3+}:Ar^{4+} = 69:28:3:0.03, after the subtraction of the anticipated valence photoionization contribution and by assuming a 70% electron detection efficiency. This branching ratio agrees reasonably well with the value (Ar^+:Ar^{2+}:Ar^{3+}:Ar^{4+} = 66:30:4:0.2) deduced from the partial cross section curves obtained by mass spectrometry [5], except for the minor Ar^{4+} contribution.

As estimated from the coincidence yields, the RDA intensity includes ~60% contribution from the cascade processes in which the filling of the initial core holes produces a single Auger electron and a second electron emission is due to the decay of excited Ar^+. On the viewpoint of the decay nature of the core hole, the contribution can be regarded as single Auger emission. Similarly, the RTA intensity includes ~40% contribution from the cascade processes in which two Auger electrons are emitted at the filling of the initial core hole. Thus, if we consider the number of Auger electrons emitted only at the filling of the initial core hole, the intensity ratio of the single Auger emission and two Auger emissions is determined to 86:12. Here, the ratio is close to the ratio (90.1:9.9 [4]) between single and double Auger decays of the $2p$ core hole. This fact suggests that the decay nature of the core hole mostly dominates the initial electron emissions and the Rydberg electron favorably behaves as a spectator. However, the large internal energies given by the spectator Rydberg electron induced subsequent electron emission after the decay of the core hole, and the subsequent processes result in the final charge state distribution which is not a mimic of the one due to the normal Auger decay.

IV. CONCLUSIONS

The resonant multiple Auger decay at the $2p_{3/2}^{-1}$ $4s$ resonance state in Ar has been investigated with a multielectron coincidence method. The energy correlation information enables us to identify cascade and direct processes in the resonant multiple Auger decays. The cascade processes result from the spectator behavior of the Rydberg electron in the first step of the core-hole decay and the subsequent electron emission due to the large internal energies of the Ar ions created in the first step of the decay. The cascade paths are the main source of the different ion charge distribution in the normal and resonant multiple Auger decays. As for direct processes, the present observation implies that the participator contributions become important as the number of the emitted electrons increases. In other words, a participation of the Rydberg electron more effectively yields multiple Auger electron emission than the sole decay of the core hole would predict.

ACKNOWLEDGMENTS

We are grateful to the Photon Factory staff for the stable operation of the PF ring. Financial support from JSPS (Grant No. 18540399) and CNRS (PICS No. 5364) are acknowledged. This work was performed with the approval of the Photon Factory Program Advisory Committee (Proposals No. 2006G230 and No. 2008G519).

[1] M. J. van der Wiel and G. Wiebes, Physica **53**, 225 (1971).
[2] T. Hayaishi, Y. Morioka, Y. Kageyama, M. Watanabe, I. H. Suzuki, A. Mikuni, G. Isoyama, S. Asaoka, and M. Nakamura, J. Phys. B **17**, 3511 (1984).
[3] H. Aksela, J. Electron Spectrosc. Relat. Phenom. **72**, 235 (1995).
[4] N. Saito and I. H. Suzuki, J. Phys. Soc. Jpn. **66**, 1979 (1997).
[5] J. A. R. Samson, W. C. Stolte, Z. X. He, J. N. Cutler, and D. Hansen, Phys. Rev. A **54**, 2099 (1996).
[6] J. H. D. Eland, O. Vieuxmaire, T. Kinugawa, P. Lablanquie, R. I. Hall, and F. Penent, Phys. Rev. Lett. **90**, 053003 (2003).
[7] Y. Hikosaka, P. Lablanquie, F. Penent, P. Selles, T. Kaneyasu, E. Shigemasa, J. H. D. Eland, and K. Ito, Phys. Rev. A **80**, 031404(R) (2009).
[8] K. Ito, F. Penent, Y. Hikosaka, E. Shigemasa, I. H. Suzuki, J. H. D. Eland, and P. Lablanquie, Rev. Sci. Instrum. **80**, 123101 (2009).
[9] H. Aksela, S. Aksela, H. Pulkkinen, G. M. Bancroft, and K. H. Tan, Phys. Rev. A **37**, 1798 (1988).
[10] J. Mursu, H. Aksela, O.-P. Sairanen, A. Kivimäki, E. Nõmmiste, A. Ausmees, S. Svensson, and S. Aksela, J. Phys. B **29**, 4387 (1996).
[11] P. Lablanquie, L. Andric, J. Palaudoux, U. Becker, M. Braune, J. Viefhaus, J. H. D. Eland, and F. Penent, J. Electron Spectrosc. Relat. Phenom. **156–158**, 51 (2007).
[12] NIST Atomic Spectra Database (version 3.1.5), available at http://physics.nist.gov/asd3